X-611-67-592

NASA TM X-63093

FIELD ALIGNED ELECTRON BURSTS AT HIGH LATITUDES OBSERVED BY OGO-4

R. A. HOFFMAN
D. S. EVANS

DECEMBER 1967

N68-17072 (ACCESSION NUMBER)
43 (PAGES)
TMX-63093 (NASA CR OR TMX OR AD NUMBER)
1 (THRU)
09 (CODE)
(CATEGORY)
FACILITY FORM 602

NASA
GODDARD SPACE FLIGHT CENTER
GREENBELT, MARYLAND

X-611-67-592

FIELD ALIGNED ELECTRON BURSTS AT HIGH LATITUDES OBSERVED BY OGO-4

R. A. Hoffman
D. S. Evans

December 1967

GODDARD SPACE FLIGHT CENTER
Greenbelt, Maryland

ABSTRACT

In a series of passes in the northern high latitude region, short bursts of radiation were observed in the energy range 0.7 to 24 kev by detectors aboard the polar orbiting satellite OGO-4. Among these bursts were a number in which the pitch angle distributions at 2.3 kev displayed a maximum at small angles to the magnetic field lines. From the distributions and energy spectra it is argued that a possible source mechanism for these particles is electric fields parallel to the magnetic field lines at distances of several earth radii. The source particles would then be the ambient thermal plasma, with two markedly different temperature components, one at a few ev, from which the field aligned radiation originates, the other greater than an order of magnitude hotter, which produces the isotropic portion of the pitch angle distribution.

INTRODUCTION

While observations of low energy charged particles have been carried out in the auroral and polar cap region for some time, the source mechanisms and locations are still open to speculation. Various aspects of the particle properties have been utilized to argue for one or another process.

From the dispersion of arrival times for particles of different energies, or lack of it, the source location can be calculated, assuming that particles of all energies originated simultaneously (Evans, 1966; Bryant et al, 1967; Lampton, 1967). Source locations from within an earth radius to the tail region have been implied by the data.

From the energy spectrum of the particles, speculations on the source mechanism can be made. A fairly monoenergetic spectrum strongly indicates that the particles are energized by a process involving electrostatic fields (Evans, 1967; Albert, 1967), while a broader spectrum, monotonically decreasing with energy, probably suggests statistical processes.

Pitch angle measurements to date, both with sounding rocket and low altitude satellite detectors, have revealed little knowledge regarding the source mechanisms. In all cases recorded for electrons of energy greater than 40 kev, the distributions have been either isotropic over the upper hemisphere or peaked at local mirroring (O'Brien, 1964; McDiarmid and Budzinski, 1964; Mozer and Bruston, 1966; Fritz, 1967). The principal satellite observations in the very low energy range for electrons ($<$40 kev) have been reported by Johnson et al

(1967), who found that in none of the cases they examined did the 0° flux exceed that at 55°. It has seemed reasonable to assume that a source mechanism operating far out along the field lines will yield isotropic particle distributions at low altitudes, and if the particles undergo at least one traversal to their mirror regions, the atmospheric losses will deplete the intensities at small pitch angles.

In contrast to all the above observations, we have measured, with a very low energy auroral particles experiment aboard the OGO-4 satellite, anisotropic fluxes with maximum intensities along the magnetic field lines. Such unusual distributions do have strong implications pertaining to the source mechanism and location.

SATELLITE ORBIT

The OGO-4 satellite was launched on July 28, 1967, at 1421 U. T. into a low altitude polar orbit having an apogee of 895 km, a perigee of 409 km, and an inclination of 86°. The data upon which this report is based was received on the fourth and fifth days in orbit when the satellite orbital plane was in a dawn-dusk configuration. The data, in quick-look form from the Information Processing Division at Goddard Space Flight Center, was acquired during the passes over the northern high latitude region as indicated in Figure 1.

While the data analysis was performed with the aid of an orbit prediction based upon initial orbital elements, the accuracy was checked by one of the experiments aboard the satellite. The airglow experiment of Mrs. Edith Reed was sensitive to starlight. From the time of observation of a bright star in the

southern hemisphere and the orbital information, its location was calculated to be within 0.2° in declination of its actual position. Two sightings were made just bracketing the passes used herein. (W. B. Fowler, private communication).

The satellite was controlled in attitude such that one side of the spacecraft was always pointed towards the earth, while another major axis was constrained to the earth-satellite-sun plane.

EXPERIMENT

A detailed description of the auroral particles experiment (designated D-11A) and calibrations appears elsewhere (Hoffman and Evans, 1967). The important features will be described here. It contains eight detectors, each comprised of an electrostatic analyzer and a channel electron multiplier. Four of these detectors look radially away from the earth (0°), while three others are positioned 30°, 60° and 90° respectively to the earth radius vector. (See Figure 2) Since the inclination of the earth's magnetic field is nearly 90° in the high latitude regions, the angles are nearly the pitch angles of the particles detected. The eighth detector is a background detector, which measured essentially no particles in the region of interest here.

The bandpass of each detector was +19%, -13% of the center energy E_0, and its angular response was about ±3° by ±7°, with the narrower angle being primarily the range of pitch angles observed, since the minor axis of the viewing cone usually lay close to the plane containing the detector axis and magnetic field. Each of the four detectors at 0° measured particles of different energies:

0.7, 2.3, 7.4, and 23.8 kev, while those at the other angles measured particles of the same energy, 2.3 kev, which was common to one of the energies sampled by a 0° detector.

The geometric factor of each detector is about 6×10^{-5} cm^2-ster at the peak of the energy passband.

A summary of the detector properties appears in Table 1.

A most important feature of the experiment is its data sampling scheme, also shown schematically in Figure 2. The outputs of the four detectors at 0° are accumulated into four logarithmic accumulators over precisely the same time interval, a half of a telemetry main frame. This is followed by the storage of the outputs of the four 2.3 kev angle detectors for precisely the same duration, a half of a main frame. As will become apparent from the presentation of the data, this simultaneity of sampling is absolutely necessary in order to properly interpret the data.

In the presentation of the data, the 2.3 kev detector at 0° will be treated as though it were two detectors, one common to the set of four detectors measuring the four energies at 0°, the other common to the set of four detectors measuring 2.3 kev particles at four pitch angles.

The counting rate data from a detector will be shown as a continuous histogram, with each bar representing the rate during a single accumulation period of a half a main frame, and with the bars adjacent to each other. In reality, however, each bar should be isolated by a blank space of equal length

in time, representing the other half a main frame during which no accumulation from the particular detector takes place.

It is the pitch angle measurements which will be emphasized in this report. While the spectral measurements at 0° are important, they can only indicate the gross features of the spectrum because of the sparcity of the points sampled on the energy scale.

DATA EXAMPLES

For the period of time sampled, and the geophysical activity present, the passes through the northern high latitude region exhibited the following characteristics: A. While crossing the dusk side auroral zone, some small, varied fluxes were observed. B. The dusk polar region was usually rather quiet, with activity picking up as the satellite moved poleward. This activity was in the form of bursts of electrons, from less than one to 10 seconds in duration, of highly variable spectra and pitch angle distributions. The activity reached a maximum in the region of highest latitude, and quieted as the satellite moved south towards the dawn auroral zone. C. In the region of the dawn auroral zone, quiet bands of electrons of several degrees width were crossed. Only the burst activity, B, will be discussed.

An example of this activity in the midnight region appears in Figure 3, as measured during revolution 54 by the 0.7 and 2.3 kev detectors at 0°. A noticeable feature of this radiation is the lack of correlation between the intensities of electrons of the two energies, although the flux at 0.7 kev was always fairly

large whenever the spikes at 2.3 kev appeared. During the bursts at 2.3 kev, the 7.4 kev detector counting rate was usually two orders of magnitude lower except for one intense burst marked on the figure. In this burst the 7.4 kev flux exceeded the 2.3 kev flux by a factor of 6, and the 0.7 kev flux by 30%. Note that the intensities at these lower energies showed little change during this higher energy burst.

The measurements at the four angles, 0°, 30°, 60° and 90°, are shown in Figure 4 for the first two bursts at 2.3 kev appearing in the previous figure. In the northern hemisphere where the field inclination is greater than about 80°, one of the solar cell paddles of the spacecraft shields a considerable portion of the cone of acceptance of the 90° detector, so in general the data from this detector should be looked upon with askance, since corrections have not been applied. While the first burst was fairly isotropic, the second burst, which was extremely broad, had a very large anisotropy until near its end. In fact at the center of the burst, the 0° detector showed a factor of two additional increase, while the other detectors displayed a minimum. The pitch angle distributions for the four time periods labeled 1 to 4 on Figure 4 are shown in Figure 5. The pitch angles have been calculated from the known inclination and declination of the magnetic field.

Because of the order of magnitude fluctuations in the 0.7 kev electron flux during the 2.3 kev electron bursts, any display of energy spectra would be meaningless. At times the 0.7 kev flux was over an order of magnitude larger

than that at 2.3 kev, and at other times the 2.3 kev flux exceeded that at the lower energy by over a factor of two. The 7.4 kev flux was two orders of magnitude lower than that at 0.7 kev.

Another example of an anisotropy appeared during revolution 62 on the evening side, and is displayed in Figure 6, with the corresponding pitch angle distributions in Figure 7. Even during the first of the three bursts, which was six main frames in length, or about 2 seconds, the degree of anisotropy fluctuated widely between successive readouts. In Table 2 we show the ratio between the 0° and 60° fluxes on a frame by frame basis, as well as the ratio for the second burst, which lasted less than one main frame (0.3 sec). The third burst was quite isotropic.

The spectrum during the first burst was much harder than the spectra measured during the bursts of revolution 54, since the 7.4 kev flux on the average was only a factor of five below that at 2.3 kev. However, again on a frame by frame basis the spectrum fluctuated widely. The ratio of the fluxes at 0.7 and 2.3 kev is also tabulated in Table 2. The short burst marked "2" in Figure 6 occurred primarily during the storage time for the angle detectors, so that the spectrum measured by the four energy detectors at 0° during the half main frames on either side in time does not pertain to the actual burst spectrum.

On revolution 60, during which data was acquired only on the morning side, a series of small anisotropic electron bursts having a very steep energy spectrum was observed. The angle detector responses are displayed in Figure 8, and the

average pitch angle distribution for the periods shaded black is shown in Figure 9. What is most significant concerning these bursts of radiation is the simultaneity between 0.7 and 2.3 kev electrons, for which correlations could be performed to a time scale of 34 milliseconds, a half a main telemetry frame at the 16 kbps real time telemetry rate.

Figure 10 contains plots of the 0.7 kev detector counting rate versus that of the 2.3 kev detector, with the correlation performed with three time delays for the 2.3 kev response between the accumulation periods of the two detectors. In the first case, the data was taken from both detectors during the same accumulation period; in the second case the data from the 2.3 kev detector was taken during the half main frame preceding that from the 0.7 kev detector; in the third case the 2.3 kev detector data was taken a full main frame before the 0.7 kev detector data. The first case shows that in all but perhaps one situation the increases in flux at both energies occurred simultaneously, since the slopes of the curves are positive. The third case shows that almost always the 0.7 kev electrons increase before the 2.3 kev electrons, since many negative slopes appear. For about half the increases the first case displays greater simultaneity than the second case. If we make the very tenuous assumption that the satellite detectors were measuring a temporal rather than a spatial situation, the dispersion in arrival times is less than 0.034 seconds, implying that the source location is less than 0.2 earth radius from the satellite.

The average energy spectrum of the electrons for these bursts appears in Figure 11.

During the short period of data acquisition in real time on revolution 59 in the dawn auroral zone, only small fluxes were observed except for one small burst appearing predominantly at 2.3 kev (Figure 11). This was interesting because the anisotropy in the pitch angle distribution of the burst particles, after subtracting the constant flux on either side of the burst, appeared also in the 30° detector (an actual pitch angle of 23°) rather than only in the 0° detector, at a pitch angle of $13\frac{1}{2}°$, as shown in Figure 12. Whether the maximum intensity also occurred at 23°, rather than 0°, is debatable, because of the poor counting statistics.

Thus, in summary, the data from seven passes provide the following properties of the electron burst radiation in the high latitude region:

1) Bursts of electrons have been found on the dusk side in the region of the auroral zone, in the high latitude polar region on the midnight side, and in the dawn auroral zone.

2) Some fraction of the bursts display a high degree of anisotropy, with the maximum intensities along the magnetic field line towards the atmosphere. No statistical study of the frequency of occurrance of these events has yet been undertaken, but the fact that such events can be found at all is of considerable importance. The anisotropies were contained within the local pitch angle cone of 20 to 40 degrees.

3) The anisotropies have been measured only at the energy of 2.3 kev. However, simultaneous with the bursts at this energy, bursts of electrons at 7.4 kev along the field lines were also observed, as well as much smaller fluxes at 23.8 kev. One might extrapolate to the conclusion that electrons even at the higher energies were also field aligned.

DISCUSSION AND SPECULATIONS

Due to the fact that these data have been recently acquired, few ground level measurements are available for use in determining whether any extraordinary events were occurring in the polar region simultaneously with the bursts. The Solar-Geophysical Data Report (No. 277) indicates that the period was extremely quiet. The sum of K_p for July 31 was 2+, and for Aug. 1, the sum was 11, with the fourth three hour period showing a 3+.

While many electron bursts were observed in the high latitude region, only those which exhibited the field aligned anisotropy will be discussed at length here.

It is perhaps most natural to assume at the outset that this anisotropy in the electron downflux is a direct consequence of a mechanism which energized these electrons, rather than an energization mechanism followed by a very unusual dumping mechanism which introduced the anisotropy, for example. This being the case it is necessary that these electrons are freshly accelerated, for the distinctive field aligned pitch angle distribution would not have persisted had these electrons been trapped with their mirror points so deep in the atmosphere.

The observation of such a field aligned flux at the top of the atmosphere has often been taken to mean that the particles could not have been released on the field line at large geocentric distances. This is because the confinement of these electrons to a 30° cone at the point of observation where the magnetic field was 0.6 gauss would require that these same electrons be confined in a cone only $\frac{1}{2}^\circ$ wide at a point on the field line where the field was 2×10^{-4} gauss; i.e., the geomagnetic tail. This extreme collimation has been regarded as prohibitive (McDiarmid and Budzinski, 1964).

Recently, however, Speiser (1965, 1967) has constructed a model for the energization and precipitation of auroral particles where such a collimation is an important feature. In Speiser's model charged particles are "trapped" in the neutral sheet by the very much stronger magnetic fields of the tail on either side. As these particles oscillate across the neutral sheet they are energized by a transverse (dawn to dusk) electric field. At some point along their trajectories, Speiser shows that they may escape from the neutral sheet onto tail magnetic field lines. The crucial feature of this step in the process is that the accelerated particles emerge from the neutral sheet with very small pitch angles, less than $\frac{1}{2}^\circ$ in some of Speiser's numerical examples, and thus could, in principle, produce the pitch angle distributions observed at the top of the atmosphere. Because the model produces a steady stream of electrons down the field line, the velocity dispersion argument made earlier against distant sources would be invalid.

However, in order to produce these very collimated pitch angle distributions, Speiser requires that the magnetic field in the neutral sheet be extremely weak, $10^{-2}\gamma$ in the example cited above. Sonnett, Colburn and Currie (1967) argue that magnetometer measurements from Explorer 35 suggest that the magnetic field in the neutral sheet is normally close to 1γ, a field too large for Speiser's model to display the anisotropy at the depths in the magnetosphere of the satellite.

Thus, while some mechanism akin to Speiser's may be responsible for the production of these electrons, it seems best to reserve judgment until the physical bases for the model are conclusively proven or disproven. It then is of interest to investigate alternative mechanisms. The observation of field aligned fluxes suggests that electron acceleration by parallel electric fields is a possible alternative mechanism. Therefore, let us investigate the effect of a parallel electric field on the energy and pitch angles of the particles, in light of our observations.

One has two equations with which to work (Northrop, 1963): the conservation of energy:

$$W_e = W_i + eV \tag{1}$$

where W is the kinetic energy of the particle, the subscripts "i" and "e" refer to the points of ingression into and egression from the electric field region, and V is the potential between the points; and the invariance of the magnetic moment:

$$\frac{W \sin^2 \alpha}{B} = \text{constant} \tag{2}$$

where B is the magnetic field strength and a the pitch angle.

Close field:

First consider the case where the electric field is confined to a very short length of field line and lies close to the spacecraft, so that B_i/B_e is close to one. (The acceleration occurs over a length of field line so short that grad B is neglected.) Also, $W_e = W_d$, where the subscript "d" means that a parameter is measured by the detectors. Then

$$W_i \leqslant W_d \sin^2 a_d \tag{3}$$

from equation 2. The direction of the inequality needs clarification. If the source particles have a reasonably isotropic distribution, and a maximum energy W_i*, then the particle which results in the maximum pitch angle at the satellite will have both W_i* and a pitch angle at ingression of 90°. Conversely, measuring a_d(maximum), or placing an upper limit on it, will give a measure of W_i*, and all other particles with either $W_i < W_i$*, or pitch angles at ingression less than 90°, or both, will result in pitch angles less than a_d(maximum) at the detectors. The three cases are illustrated in Figure 13.

For an $a_d \leqslant 30°$, and $W_d = 2.3$ kev, equation 3 gives $W_i \leqslant 0.6$ kev, a non-thermal energy. One then must have a source of non-thermal electrons, although it could produce an isotropic distribution. Perhaps the data indicates such an additional source is operating, because the anisotropic peaks at 2.3 kev are usually contained within, at least in time, regions of high 0.7 kev fluxes, as

shown in Figure 3. However, we can argue further: if such a non-thermal source exists for at least 0.6 kev electrons, it would not be unreasonable to assume it could produce, at times, somewhat higher energies (W_i larger). This would result in an anisotropy width in pitch angle which would sometimes be seen by both the 0° and 30° detectors, but not the 60° detector (a_d larger, since W_d is fixed by the detectors). While our search for anisotropic events has just been initiated, with only about 13 events analyzed, such a situation has been seen only for the small event of revolution 59, and shown in Figure 12.

The potential drop required to produce a few kev electrons if imposed over distances of one to a few thousand kilometers would necessitate high electric fields, in the range of one to tens of millivolts/meter. With this low altitude case, one would feel uncomfortable supporting such parallel electric fields in a region of high densities of thermal particles (the ionosphere) for periods of tens of seconds.

Extended field:

If the electric field intensity is reduced by extending the field to larger distances, the converging magnetic field affects the particle pitch angles. Then the maximum energy of the source electrons as dictated by the anisotropy measurement at 2.3 kev is

$$W_i \leq \frac{B_i}{B_d} W_d \sin^2 a_d \qquad (4)$$

If we assume that $B \overset{\alpha}{\sim} 1/D^3$, where D is geocentric distance, then

$$W_i \leqslant \left(\frac{D_d}{D_i}\right)^3 W_d \sin^2 a_d \qquad (5)$$

Figure 14 is a family of plots of W_i as a function of a_d, each curve holding $M = D_i / D_d$ (i.e., D_i) constant. If we also consider that $W_i \ll W_d$, which is true for all but the top parts of the curves for large a_d, and that the electric field intensity is constant along a line of force, then this field intensity will be a constant for each curve. Only the magnitude of the electric field depends upon the distance between the points of ingression and egression. If the latter is coincident with the altitude of the satellite, the magnitudes are those given in Figure 14. As the point of egression is moved to higher altitudes, closer to the point of ingression, the field intensity increases.

Therefore, if the ingression particles are the thermal component of the magnetosphere, with energies below a few ev, and the potential of -2.3 kV with respect to the position of the spacecraft exists at distances of three to six earth radii, the anisotropy at the satellite would be contained within pitch angles of 20° to 40°. Higher energy particles would be observed in the bursts only if the electric field extended to larger distances, and thus the potential difference from the altitude of the spacecraft to points of ingression reached the values of W_d measured by the higher energy detectors.

The situation is illustrated schematically in Figure 15. The electric field is impressed over some region along the lines of force which contains particles

of energy W_i, and passes through the satellite. Since $W_i \ll W_d$, the particles at 2.3 kev measured by the angle detectors in the satellite must have originated only at the point along the field lines where the potential was 2.3 kV. Particles originating above or below this point would have either too much or too little energy to be detected. However, if the electric field extended sufficiently far along the field line to give a potential of 7.4 kV, particles would then be detected by the 7.4 kev detector at 0°.

Electric fields of the order of 10^{-4} volts/meter are required for this extended field case.

Far fields:

Parallel electric fields confined to the tail region would require ingression energies smaller than about a half an ev to produce the desired pitch angle distribution, since in equation 4, $B_i/B_d \leq 10^{-3}$. Serbu and Maier (1966) indicate electron temperatures in the one to several ev range at large distances from the earth, although their data in the tail region were taken during what they considered to be "disturbed" periods of time. However, on the sunward side during "quiet" periods, similar thermal energies were measured at distances beyond five earth radii.

Isotropic component:

The pitch angle measurements during the bursts, especially as displayed in Figure 7, not only show a field aligned component of the radiation, but also what appears to be an isotropic component, whose temporal characteristics are

identical to those of the anisotropic particles. Because of this synchronousness, it would be reasonable to assume that the same source mechanism also produces the isotropic component.

Such a total pitch angle distribution could be caused by parallel electric fields only if the ingression energy spectrum contained a high energy tail, in which the temperatures of the two components are markedly different. These particles, with $W_i > W_i^*$ of the thermal component, would result in particles at all pitch angles at the detectors. Such a high energy tail is also observed by Serbu and Maier (1966), with its temperature greater than an order of magnitude that of the low energy component (Maier, private communication). Such differing temperatures cause a sharp inflection in the total energy spectrum being accelerated by the electric field, which displays itself as the inflection between the field aligned and isotropic portions of the pitch angle distribution.

Isotropic bursts:

Extrapolating our arguments even further, it would also seem reasonable to assume that all bursts, whether they display the field alignment characteristic or not, originate from the same source mechanism, since field aligned and isotropic bursts are seen seconds apart on the same pass. With parallel electric fields as the mechanism, the appearance of the anisotropy would depend upon the relative densities of the two energy component gas in the ingression region. Again, in terms of their electric current-voltage retardation curves, Serbu and Maier measure a variable ratio of the thermal to more energetic electrons.

During quiet conditions the ratio is generally 10 to 1 or more, while during disturbed conditions it is not greater than 5 to 1. However, in terms of densities, or particles available for acceleration, the ratio will fluctuate even greater. Thus the isotropic distribution may result from a small ratio in the ingression region, and the field aligned aspect emerges when the high energy component is suppressed.

Comparison with other experiments:

The relationship of the bursts of very low energy electrons to the bursts observed by detectors with low energy cut-offs at 10 and 40 kev will remain unknown until the study of the frequency of events in latitude and local time observed by the OGO-4 detectors can be performed. However, the same statistical studies which have been carried out with the greater than 10 kev electrons indicate a dearth of such bursts in the very high latitude region above 77° invariant latitude (Fritz and Gurnett, 1965). On the other hand the spectrum becomes softer with increasing latitude (Fritz, 1967), so that there may be simply a lack of detectable fluxes of particles above 10 kev in this region. Judging from the few passes analyzed in this study, our findings do show that the high latitude region above 80° invariant latitude is very active with regard to less than 10 kev electron precipitation.

In no way should this discussion of parallel electric fields be construed to indicate that such a mechanism is thought to be the source of the electron bombardment in the auroral zone. If such fields do indeed exist they are applicable

only to the short bursts of electrons in the low energy range observed by the detectors while the satellite is in the very high latitude region.

ACKNOWLEDGEMENTS

The assistance of Mr. Allen Thompson and Mrs. Lillian Keegan in the data processing is gratefully acknowledged. Discussions with many people, especially Drs. A. Konradi and D. J. Williams, have been beneficial in the data interpretations. We also wish to thank Mr. W. B. Fowler for the check on the accuracy of the orbit prediction utilizing data from the airglow experiment aboard the OGO-4 satellite. The cooperation of the members of the OGO Control Center, especially Messrs. J. Meenan and F. Giordano, in the daily operation of the Auroral Particles Experiment is gratefully appreciated.

REFERENCES

Albert, R. S., "Nearly monoenergetic electron fluxes detected during a visible aurora", Phys. Rev. Letters, 18, 369, 1967.

Bryant, D. A., H. L. Collin, G. M. Courtier, and A. D. Johnstone, "Evidence for velocity dispersion in auroral electrons", Nature, 215, 45-46, 1967.

Evans, D. S., "Rocket measurements of energetic electron precipitation in the auroral zone", Goddard Space Flight Center preprint, X-611-66-9, 1966.

Evans, D. S., "The observation of a near monoenergetic flux of auroral electrons", Goddard Space Flight Center preprint, X-611-67-487, 1967.

Fritz, T. A., "Spectral, spatial and temporal variations observed for outer zone electrons from 10 to 100 kev with satellite Injun 3", University of Iowa preprint, 67-42, 1967.

Fritz, T. A., and D. A. Gurnett, "Diurnal and latitudinal effects observed for 10-kev electrons at low satellite altitudes", J. Geophys. Res., 70, 2485-2502, 1965.

Hoffman, R. A., and D. S. Evans, "OGO-4 auroral particles experiment", Goddard Space Flight Center preprint, X-611-671 , 1967.

Johnson, R. G., R. E. Meyerott, and J. E. Evans, "Coordinated satellite, ground-based and aircraft-based measurements on auroras", "Aurora and Airglow, Ed. by B. M. McCormac, Reinhold Pub. Co., New York, 1967.

Lampton, M., "Daytime observations of energetic auroral zone electrons", Dept. of Physics, University of California preprint, April, 1967.

McDiarmid, I. B., and E. E. Budzinski, "Angular distributions and energy spectra of electrons associated with auroral event", Canadian J. of Physics, 42, 2048, 1964.

Mozer, F. S., and P. Bruston, "Properties of the auroral-zone electron source deduced from electron spectrums and angular distributions", J. Geophys. Res., 71, 4451, 1966.

Northrup, T. G., The Adiabatic Motion of Charged Particles, Interscience Publishers, New York, 1963.

O'Brien, B. J., "High-latitude studies with satellite Injun 3, Part 3, Precipitation of electrons into the atmosphere", J. Geophys. Res., 69, 2667-2672, 1964.

Serbu, G. P., and E. J. R. Maier, "Low-energy electrons measured on IMP-2", J. Geophys. Res., 71, 3755, 1966.

Sonnett, C. P., D. S. Colburn, and R. G. Currie, "The intrinsic magnetic field of the moon", J. Geophys. Res., 72, 5503-5507, 1967.

Speiser, T. W., "Particle trajectories in model current sheets, 1, Analytical solutions", J. Geophys. Res., 70, 4219-4226, 1965.

Speiser, T. W., "Particle trajectories in model current sheets, 2, Applications to auroras using a geomagnetic tail model", J. Geophys. Res., 72, 3919-3932, 1967.

TABLE 1

Angle	Center Energy (kev)	Efficiency* (%)	Flux Conversion Factor** (to electrons/cm^2-sec-ster-kev)
0°	0.7	80	6.70×10^5
0°	2.3	82	2.03×10^5
0°	7.4	65	8.13×10^4
0°	23.8	45	3.60×10^4
30°	2.3	82	2.03×10^5
60°	2.3	82	2.03×10^5
90°	2.3	82	2.03×10^5

*See Hoffman and Evans, 1967.

**to convert from counts/readout for the 4 kilobit/sec tape storage mode of the spacecraft. For real time telemetry at 16 kilobits/sec these factors must be multiplied by 4.

TABLE 2

Main Frame	Flux Measured by 0° Detector / Flux Measured by 60° Detector	At 0° Flux in 2.3 kev Detector / Flux in 7.4 kev Detector
1	3.97	46
2	1.51	86
3	0.91	1.0
4	1.71	1.6
5	2.26	4.6
6	2.53	3.5
Second burst	3.54	—

FIGURE CAPTIONS

Figure 1. Orbit of the OGO-4 satellite in invariant latitude as a function of local time for the revolutions from which data has been analyzed. The heavier portions of the lines indicate the regions where data examples have been taken.

Figure 2. Schematic diagram of the experiment detector system indicating the look directions of the detectors with respect to the earth radius vector, the center energies measured by the detectors, and the sampling scheme of the detector outputs.

Figure 3. An example of burst activity in the midnight region, as seen during revolution 54 (4 kbps data).

Figure 4. Counting rates of the four detectors with common center energy of 2.3 kev and angles with respect to the radius vector from the earth of 0°, 30°, 60° and 90° during revolution 54 (4 kbps data).

Figure 5. Pitch angle distributions of bursts during revolution 54.

Figure 6. Same as Figure 3, for revolution 62 (4 kbps data).

Figure 7. Pitch angle distributions of bursts during revolution 62.

Figure 8. Same as Figure 3, for revolution 60 (16 kbps data).

Figure 9. Average pitch angle distribution of bursts during revolution 60.

Figure 10. Correlation determination between 0.7 and 2.3 kev electrons for bursts during revolution 60.

Figure 11. Average energy spectrum measurements for bursts during revolutions 60 and 59.

Figure 12. Pitch angle distribution of burst during revolution 59.

Figure 13. Illustration of the fact that a measurement of the maximum pitch angle of the anisotropy defines the maximum energy of the ingression particles.

Figure 14. Maximum energy of the ingression particles consistent with the maximum extent in pitch angle of the field aligned radiation for various ingression distances given by $M = D_i / D_d$ (see equation 5 and text following).

Figure 15. Illustration of the effect of a parallel electric field impressed along a tube of force containing thermal particles with a maximum energy W_i * as well as a high energy tail.

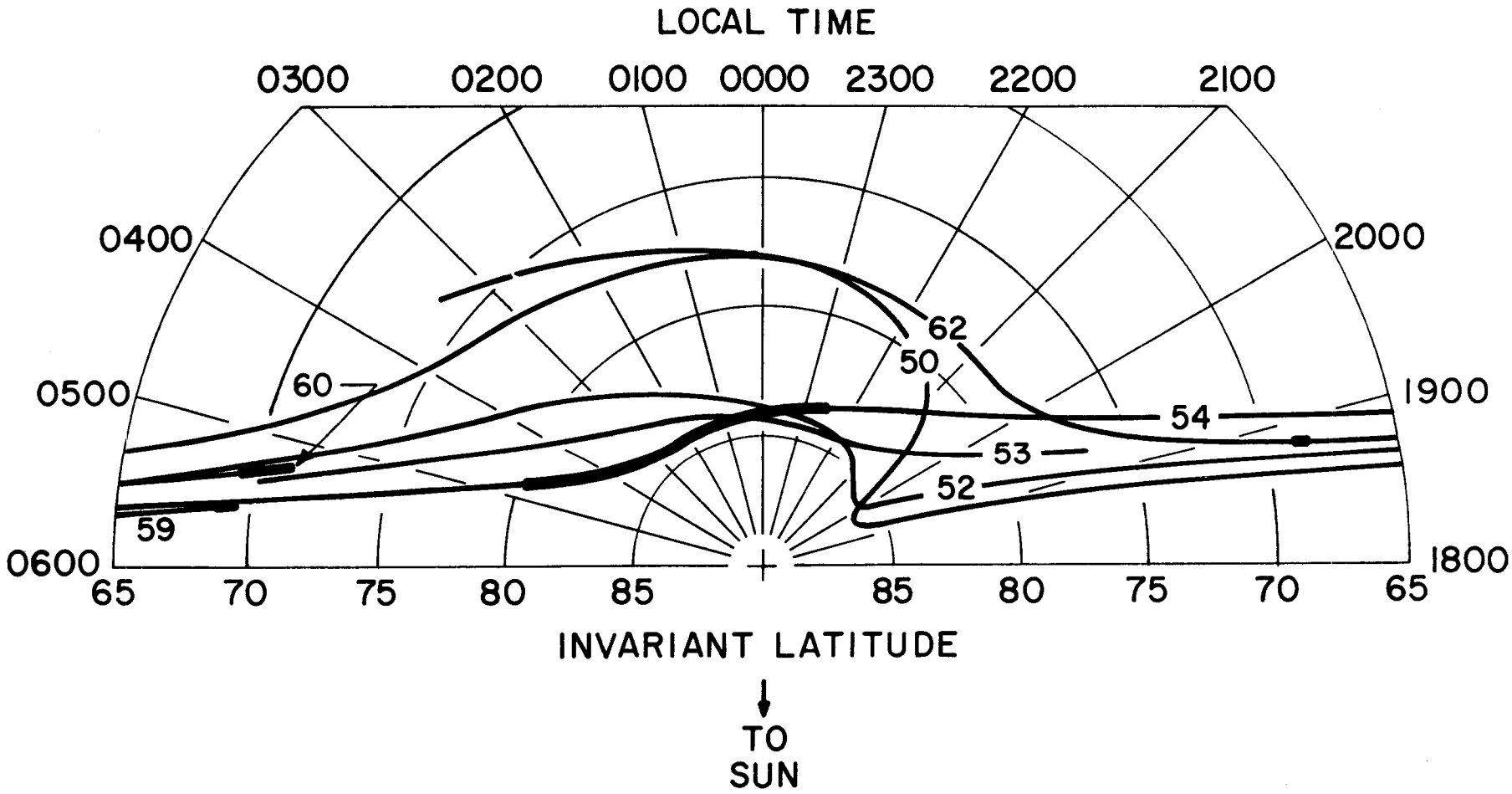
LOCAL TIME
0300
0200
0100
0000
2300
2200
2100
0400
2000
0500
1900
0600
1800
65
70
75
80
85
85
80
75
70
65
62
50
60
54
53
52
59
INVARIANT LATITUDE
TO
SUN

Figure 1

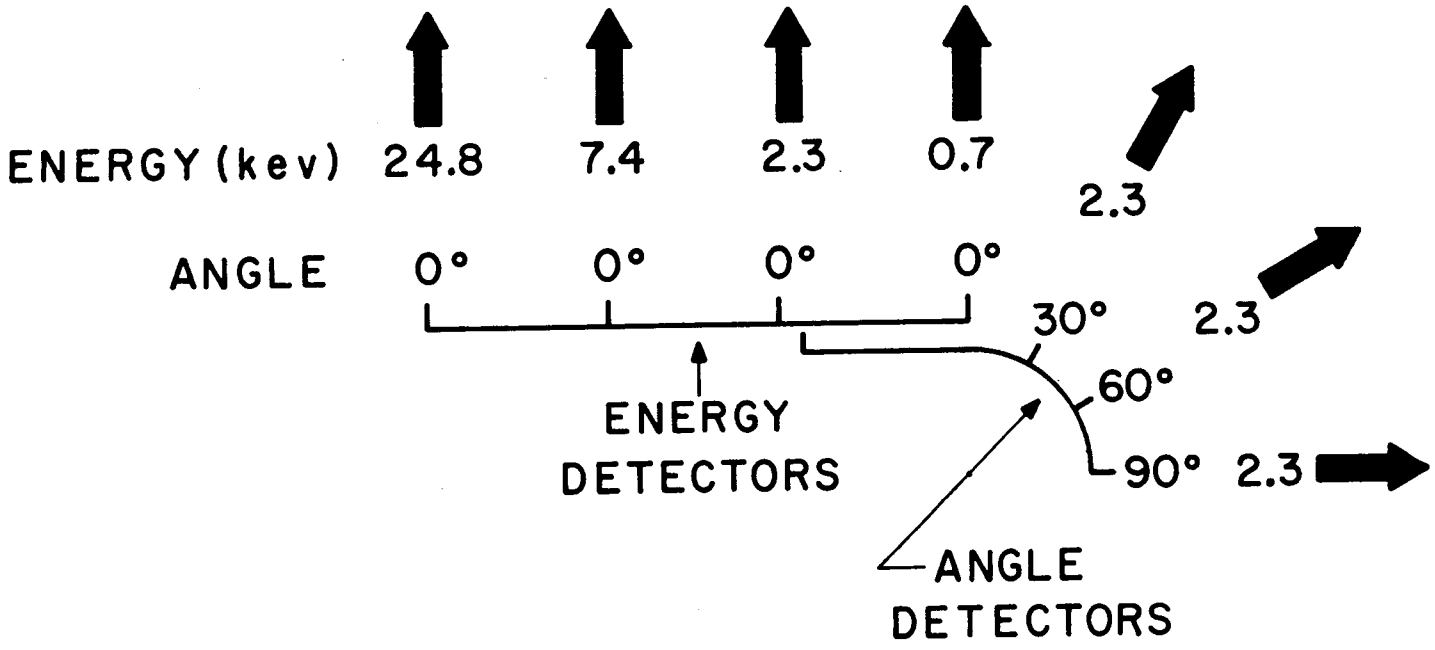
ENERGY (kev)
24.8
7.4
2.3
0.7
2.3
ANGLE
0°
0°
0°
0°
30°
2.3
60°
90°
2.3
ENERGY DETECTORS
ANGLE DETECTORS

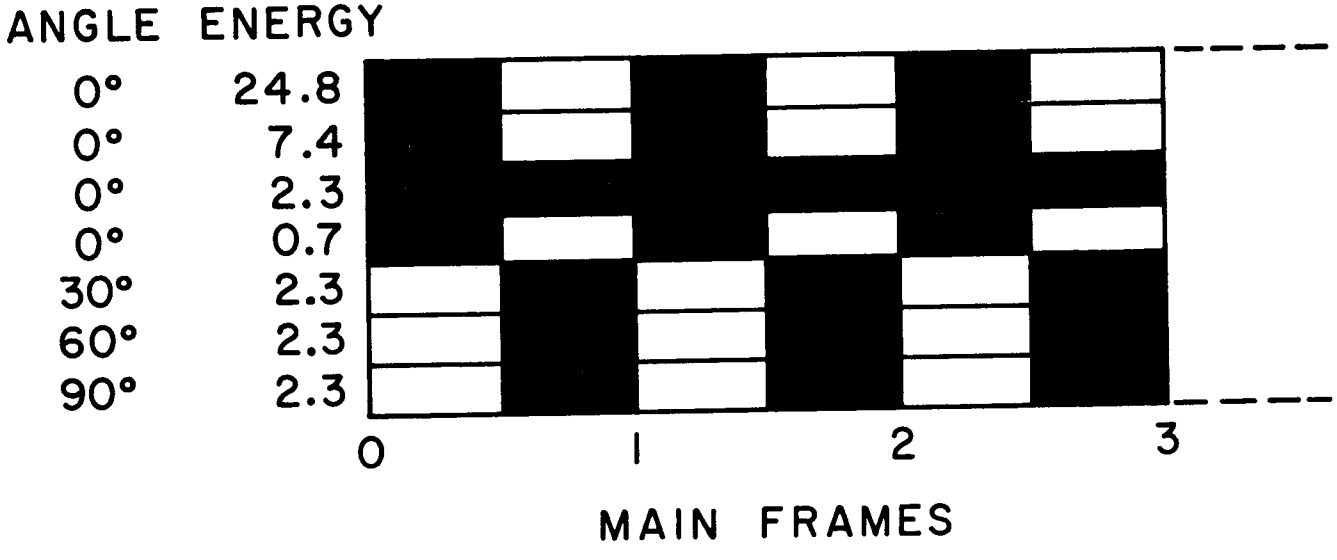
ANGLE
ENERGY
0°
24.8
0°
7.4
0°
2.3
0°
0.7
30°
2.3
60°
2.3
90°
2.3
0
1
2
3
MAIN FRAMES

Figure 2

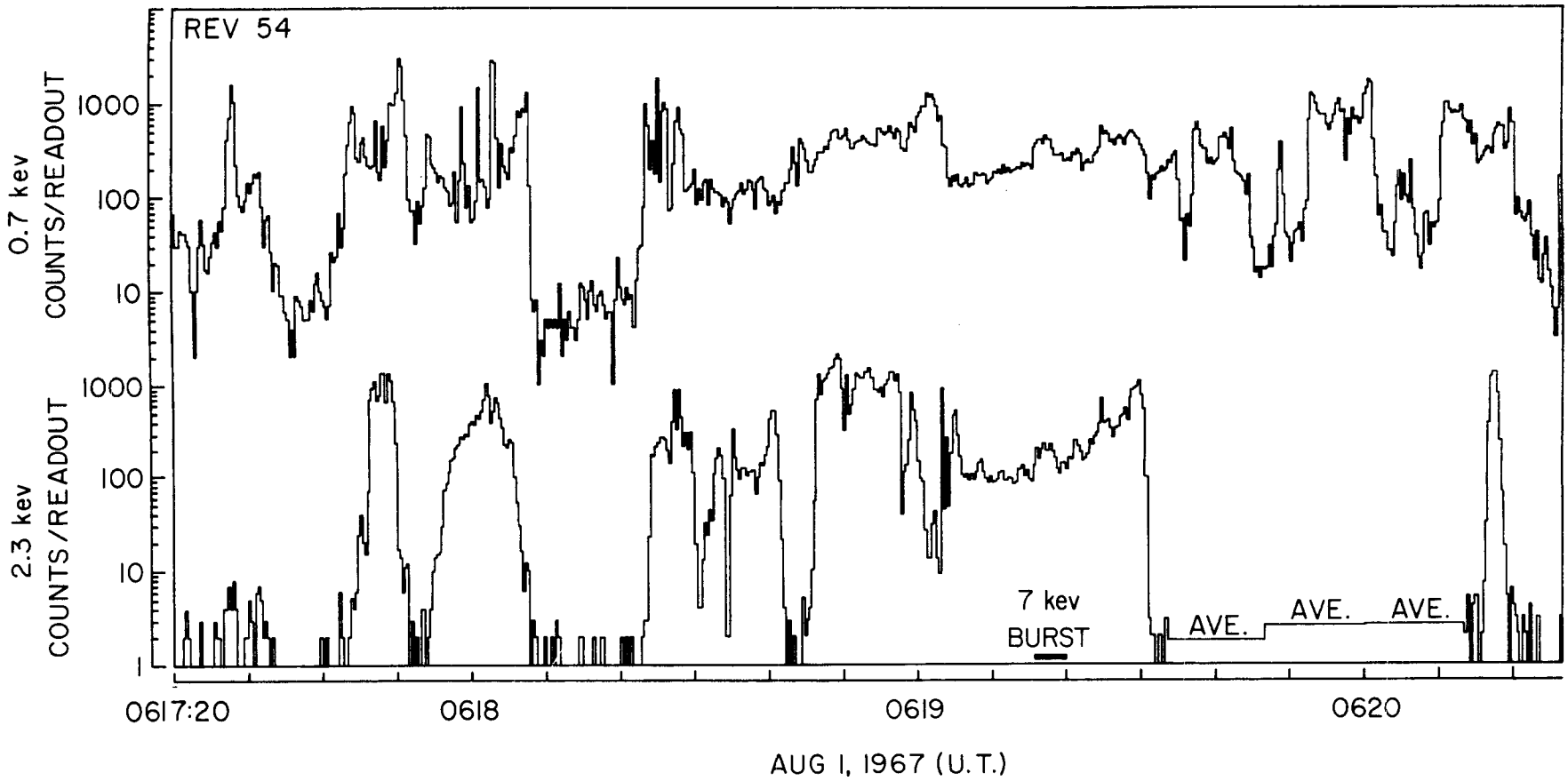
REV 54
0.7 kev
COUNTS/READOUT
1000
100
10
2.3 kev
COUNTS/READOUT
1000
100
10
1
7 kev
BURST
AVE.
AVE.
AVE.
0617:20
0618
0619
0620
AUG 1, 1967 (U.T.)

Figure 3

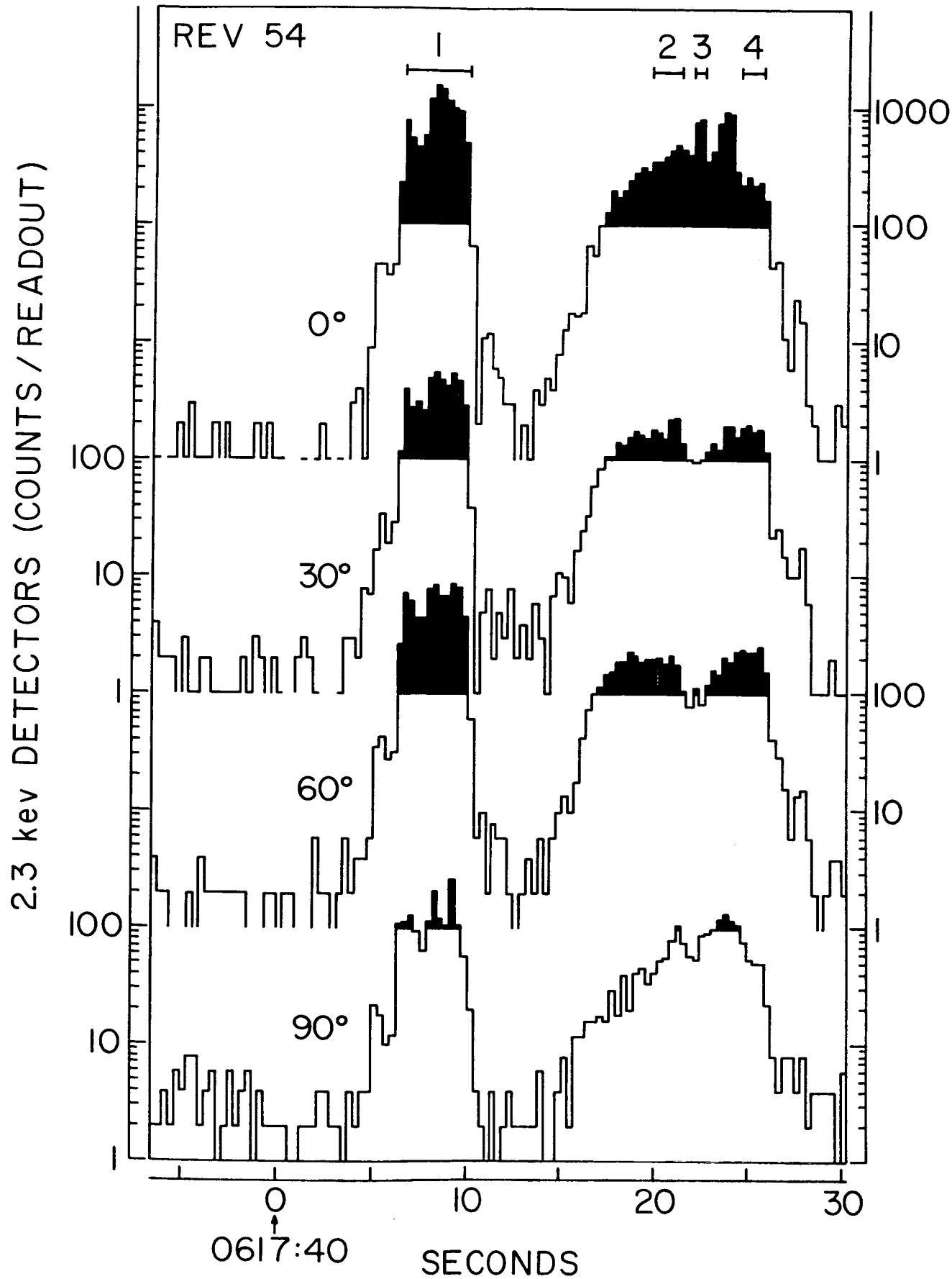
REV 54
1
2 3 4
0°
30°
60°
90°
2.3 kev DETECTORS (COUNTS / READOUT)
1000
100
10
1
100
10
1
100
10
1
0
10
20
30
0617:40
SECONDS

Figure 4

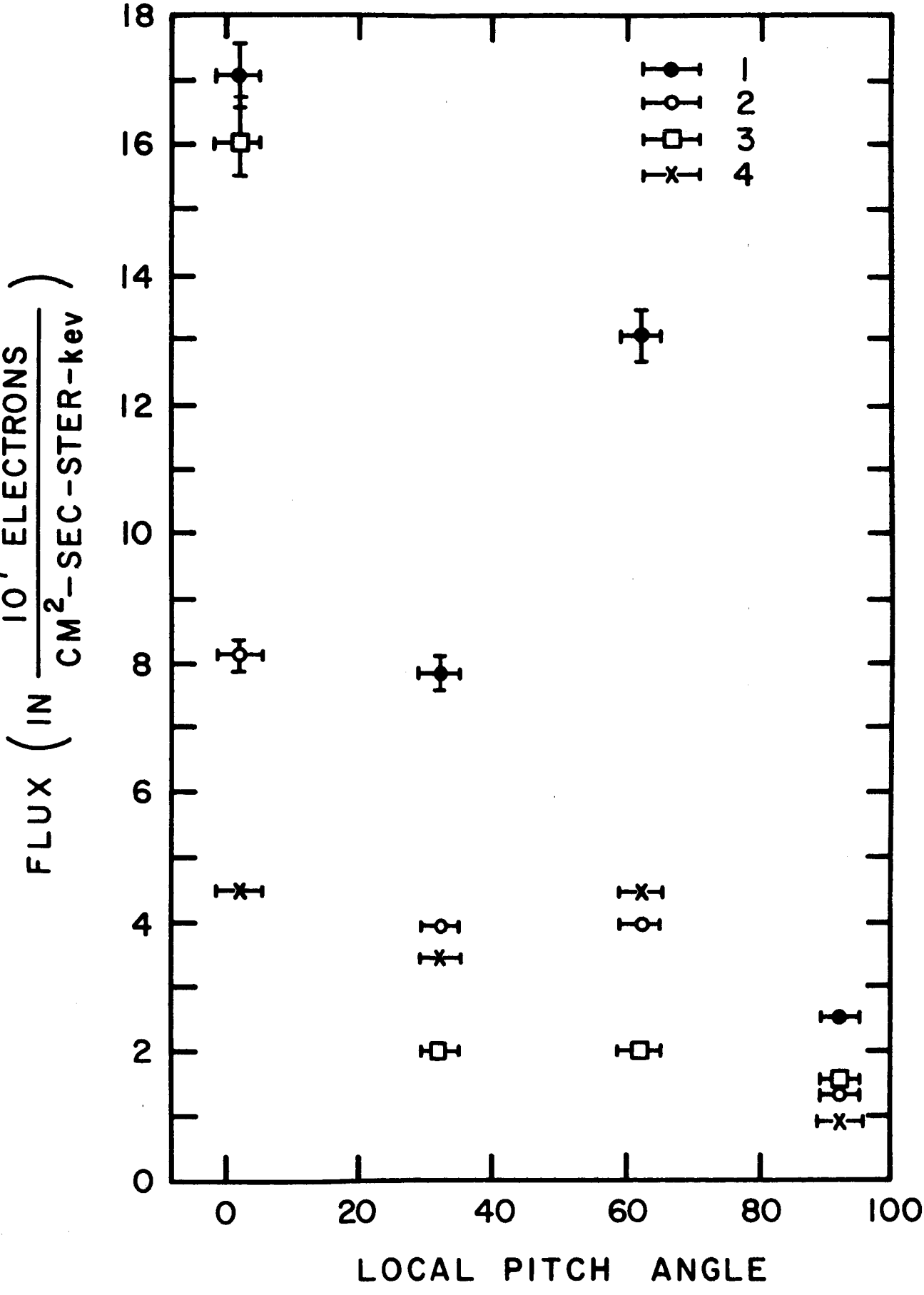
FLUX (IN $\frac{10^7 \text{ ELECTRONS}}{\text{CM}^2\text{-SEC-STER-kev}}$)
LOCAL PITCH ANGLE
0
2
4
6
8
10
12
14
16
18
0
20
40
60
80
100
1
2
3
4

Figure 5

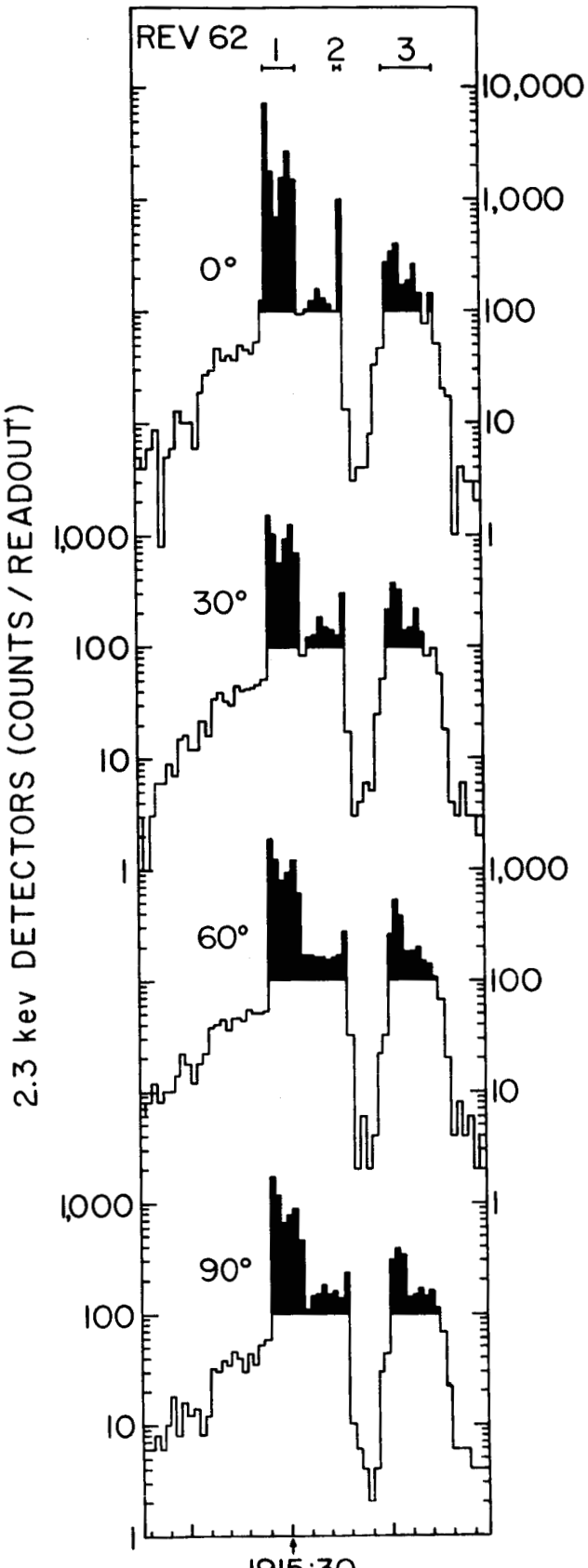
REV 62
1
2
3
10,000
1,000
100
10
1
0°
30°
60°
90°
2.3 kev DETECTORS (COUNTS / READOUT)
1915:30
SECONDS

Figure 6

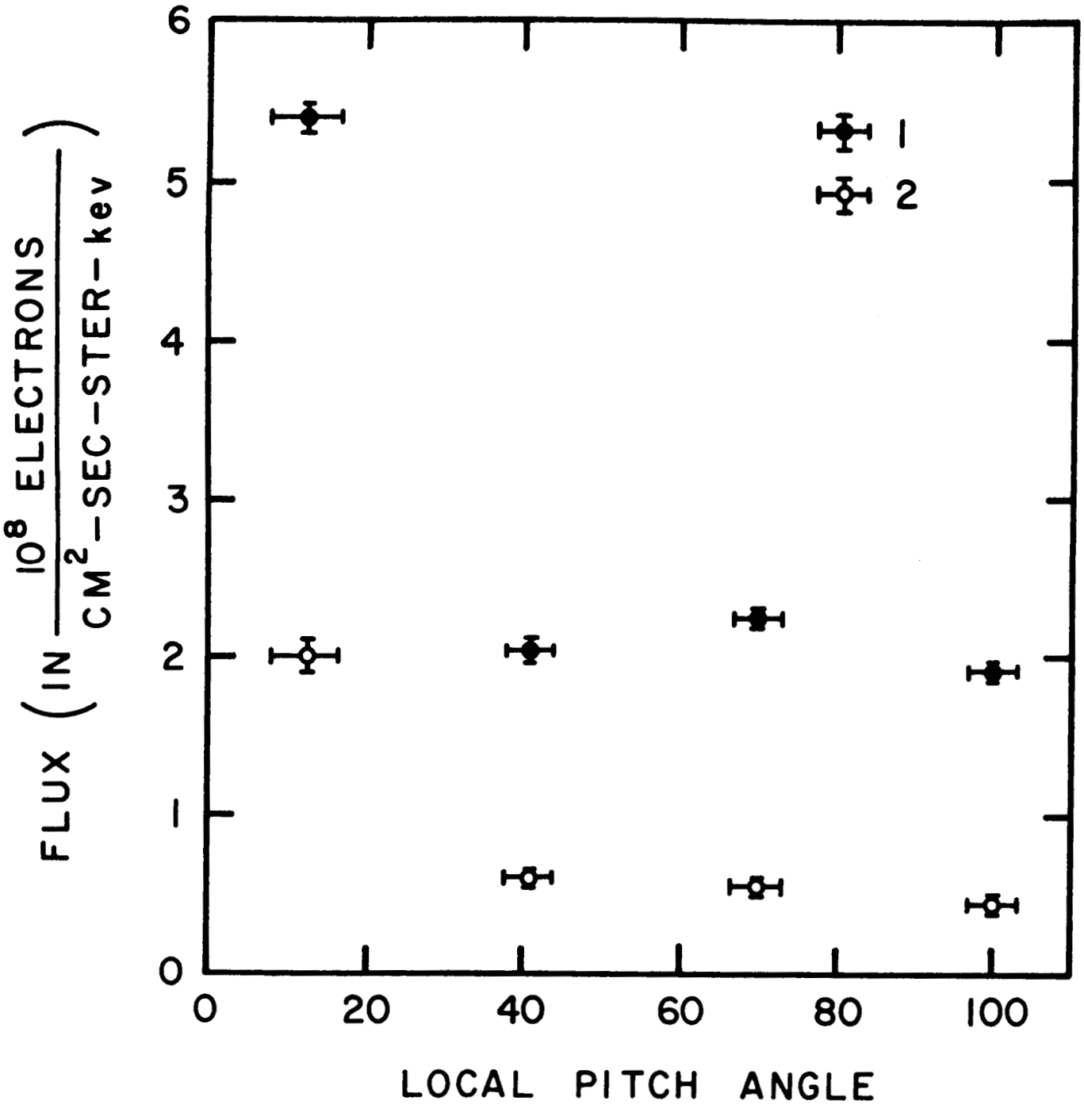
FLUX (IN $\frac{10^8 \text{ ELECTRONS}}{\text{CM}^2\text{-SEC-STER-kev}}$)
LOCAL PITCH ANGLE
0
20
40
60
80
100
0
1
2
3
4
5
6
1
2

Figure 7

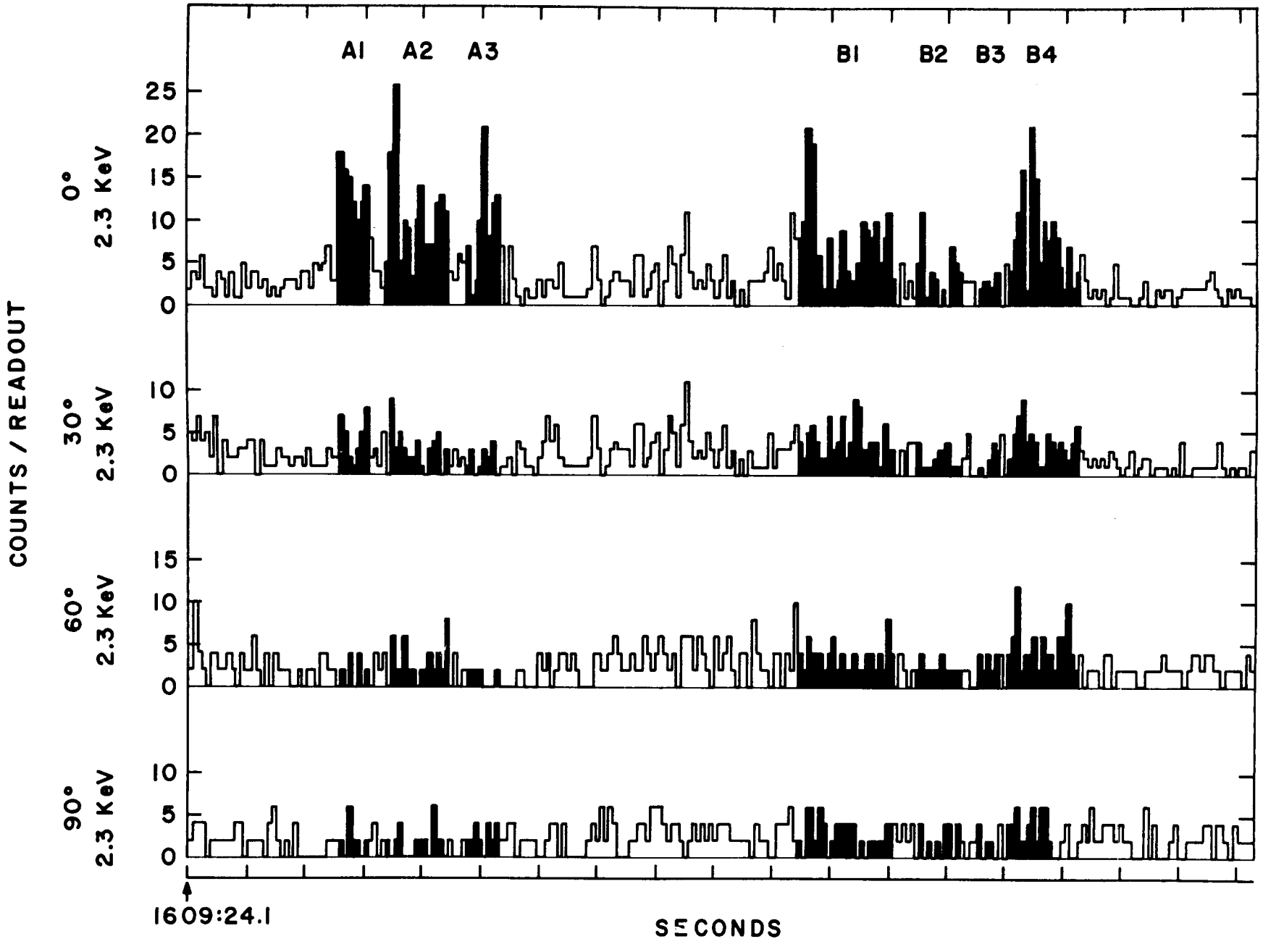
A1
A2
A3
B1
B2
B3
B4
0°
2.3 KeV
30°
2.3 KeV
60°
2.3 KeV
90°
2.3 KeV
COUNTS / READOUT
1609:24.1
SECONDS

Figure 8

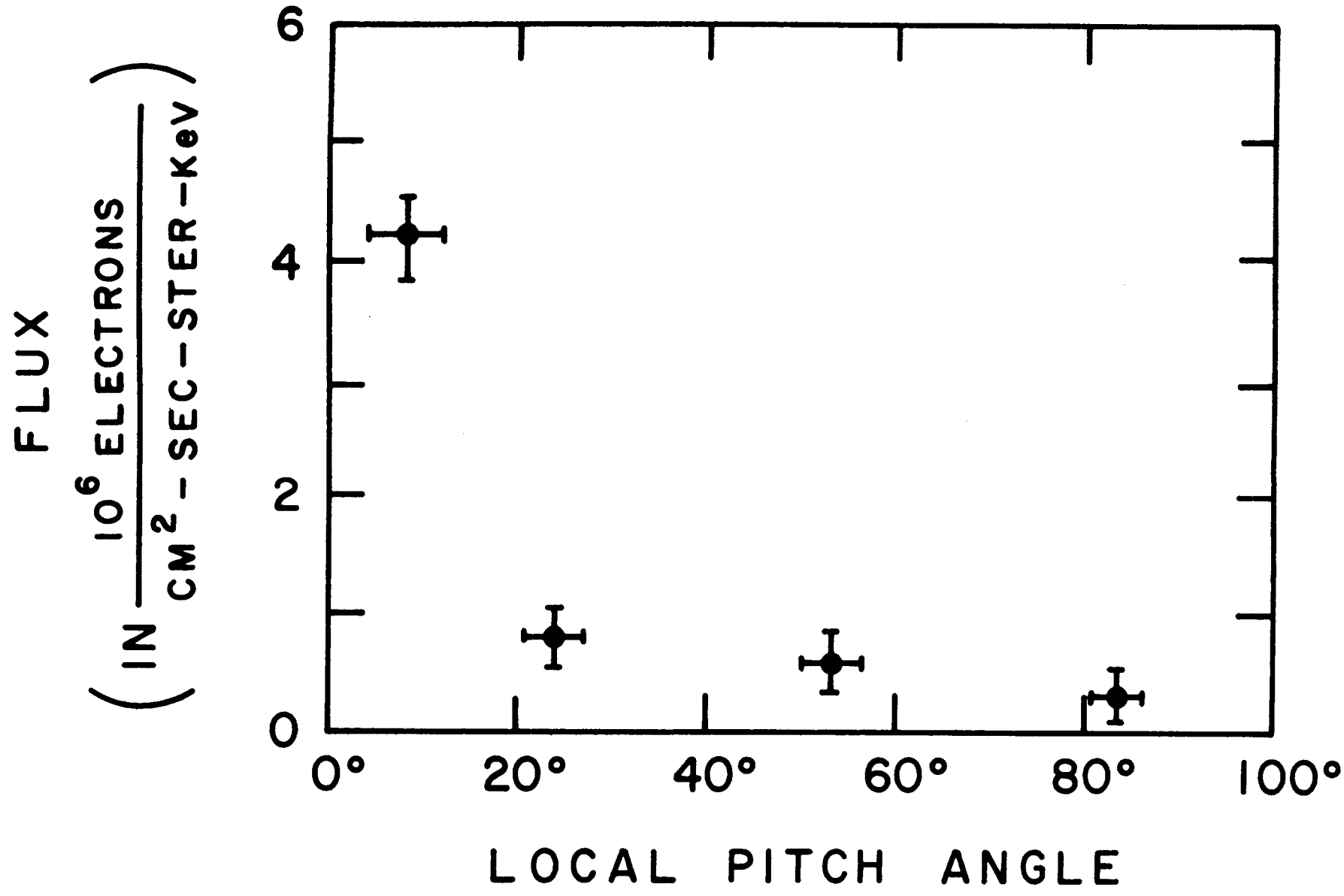
FLUX
$\left(\text{IN } \frac{10^6 \text{ ELECTRONS}}{\text{CM}^2 - \text{SEC} - \text{STER} - \text{KeV}}\right)$
6
4
2
0
0°
20°
40°
60°
80°
100°
LOCAL PITCH ANGLE

Figure 9

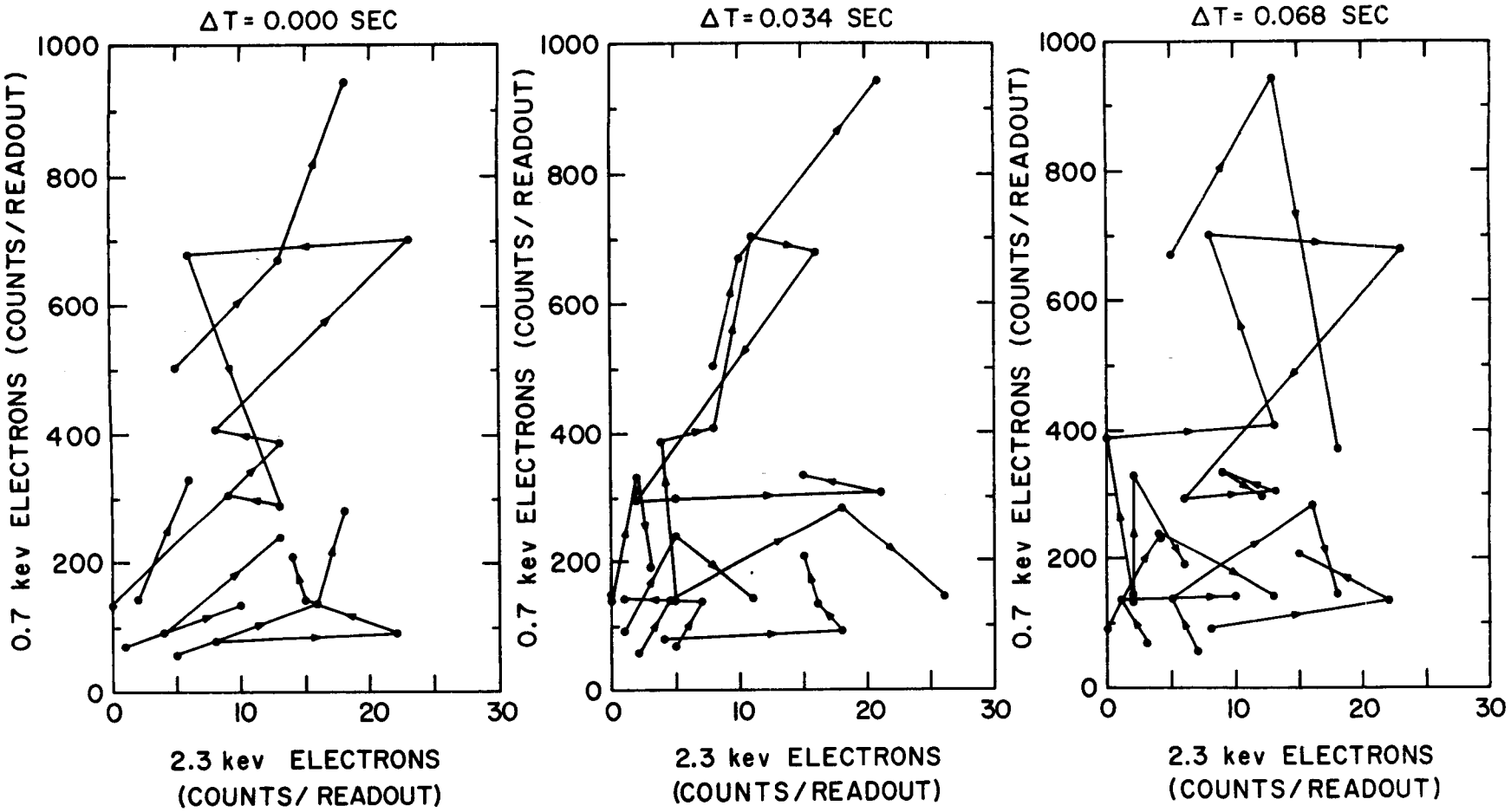
ΔT = 0.000 SEC
ΔT = 0.034 SEC
ΔT = 0.068 SEC
0.7 kev ELECTRONS (COUNTS/READOUT)
2.3 kev ELECTRONS (COUNTS/READOUT)
0
200
400
600
800
1000
0
10
20
30

Figure 10

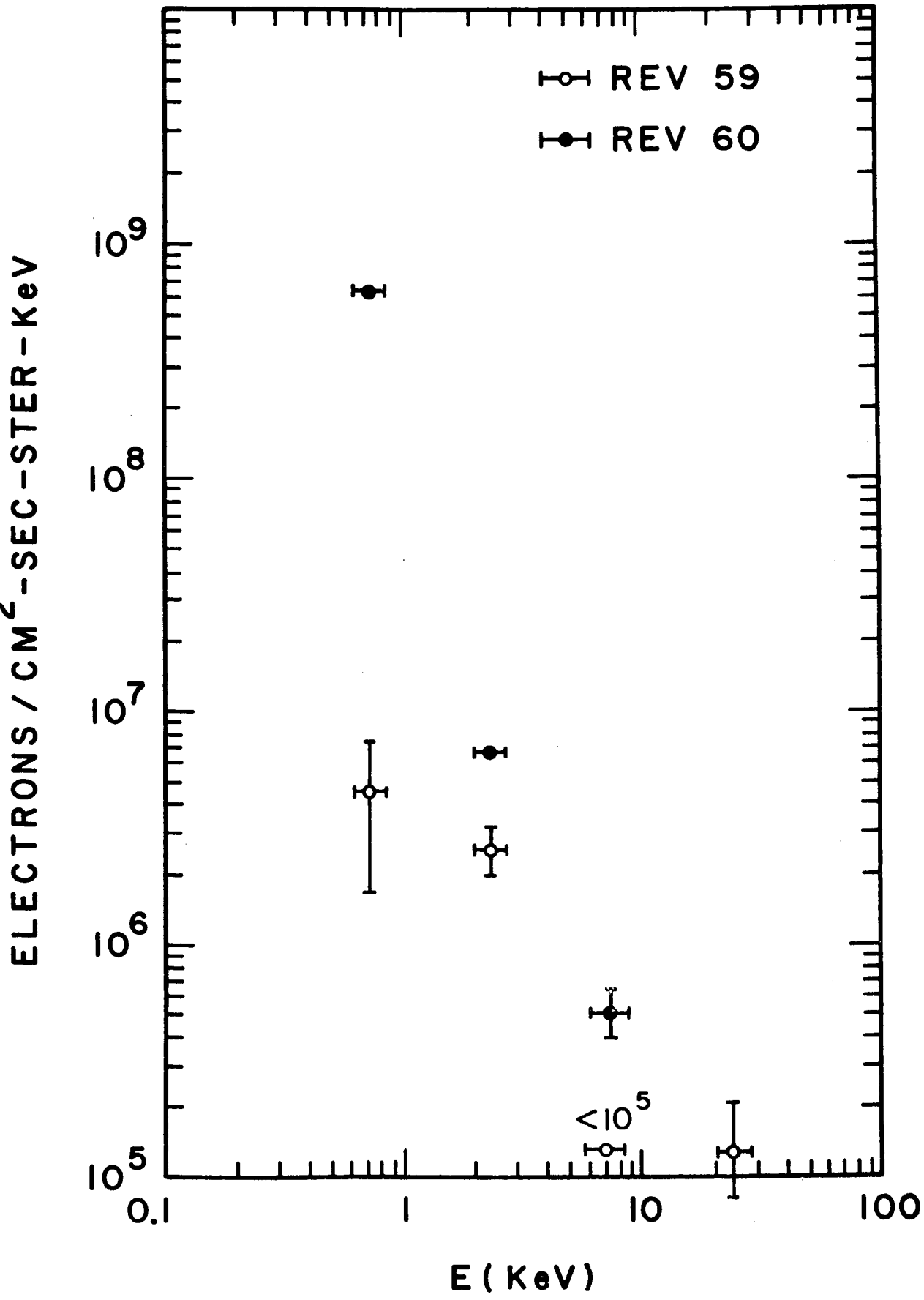
REV 59
REV 60
ELECTRONS / CM^2-SEC-STER-KeV
10^9
10^8
10^7
10^6
10^5
$<10^5$
0.1
1
10
100
E (KeV)

Figure 11

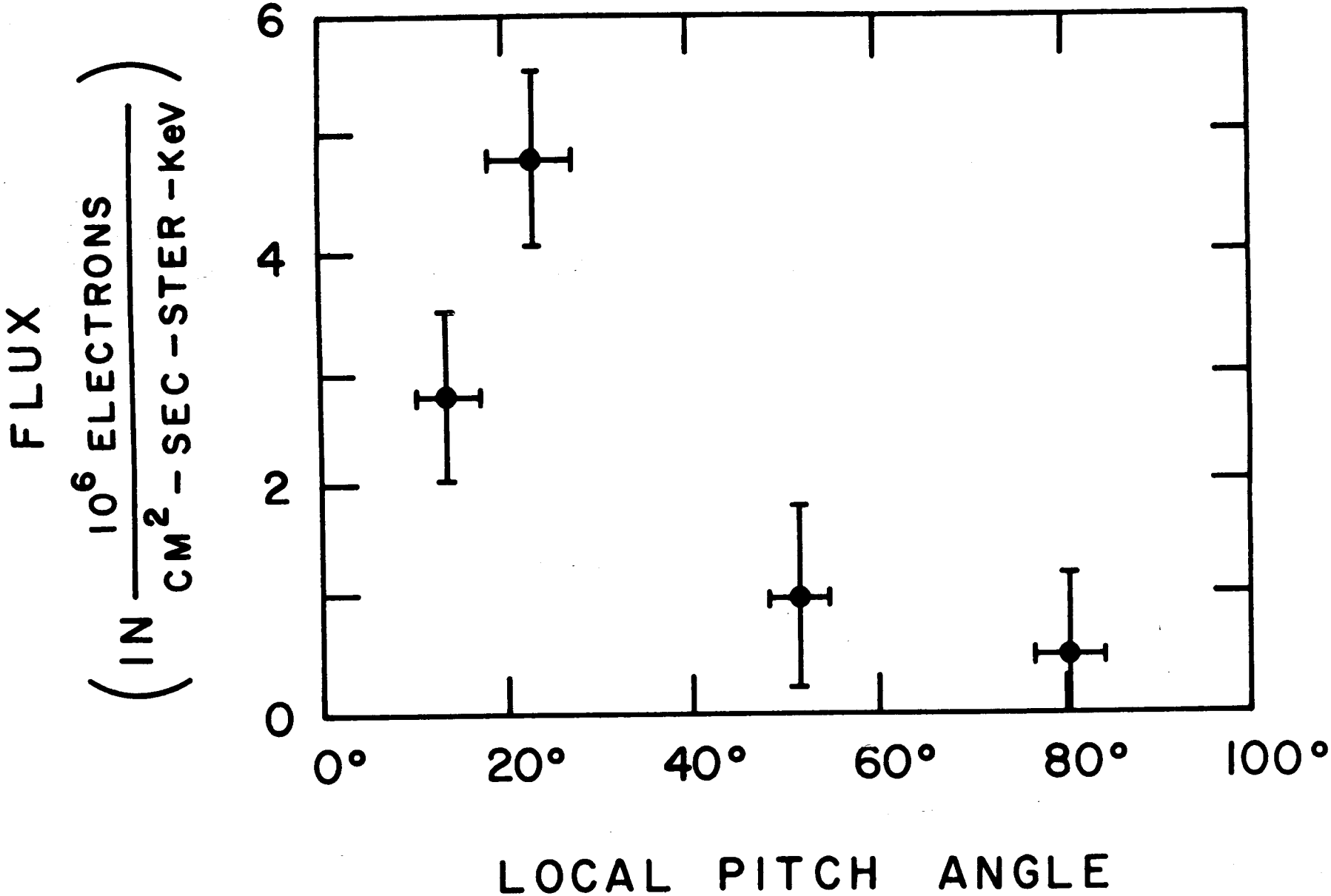
FLUX
$\left(\text{IN } \frac{10^6 \text{ ELECTRONS}}{\text{CM}^2 - \text{SEC} - \text{STER} - \text{KeV}}\right)$
6
4
2
0
0°
20°
40°
60°
80°
100°
LOCAL PITCH ANGLE

Figure 12

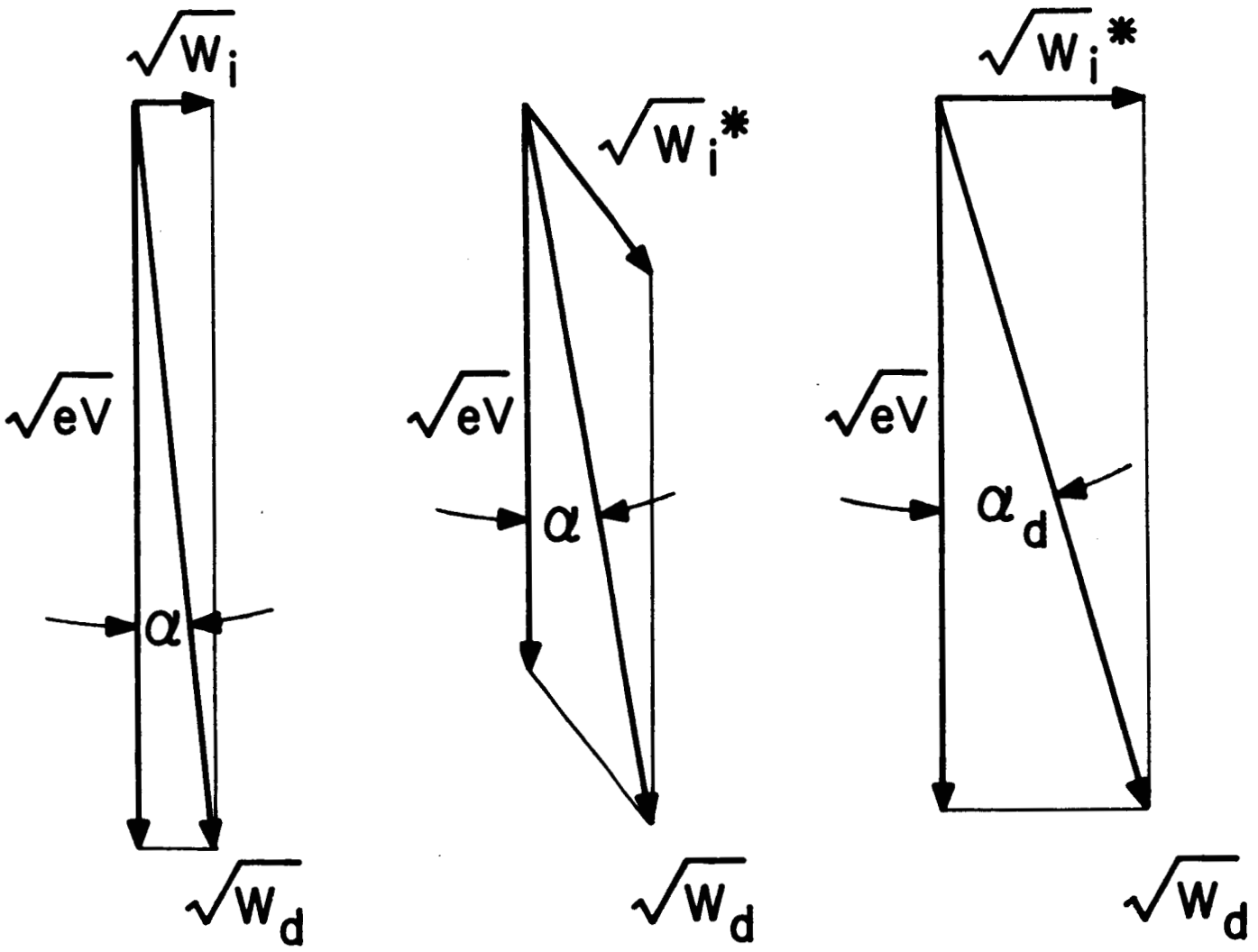

W_d = CONSTANT (MEASURED)

$W_i < W_i^*$	$W_i = W_i^*$	$W_i = W_i^*$
$\alpha_i = 90°$	$\alpha_i < 90°$	$\alpha_i = 90°$
$\alpha < \alpha_d$	$\alpha < \alpha_d$	$\alpha = \alpha_d$

Figure 13

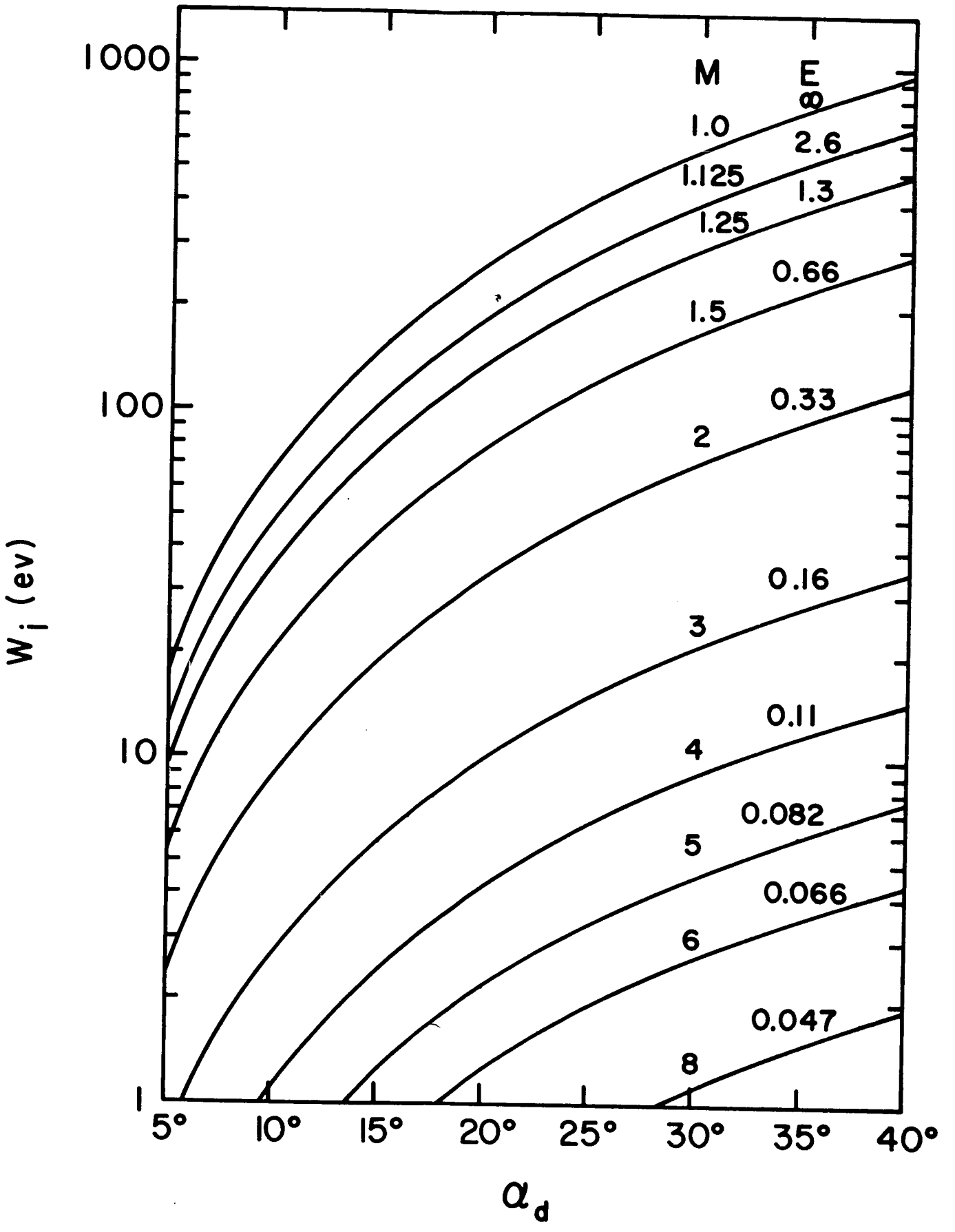
1000
100
10
1
W_i (ev)
M
E_∞
1.0
2.6
1.125
1.3
1.25
0.66
1.5
0.33
2
0.16
3
0.11
4
0.082
5
0.066
6
0.047
8
5°
10°
15°
20°
25°
30°
35°
40°
α_d

Figure 14

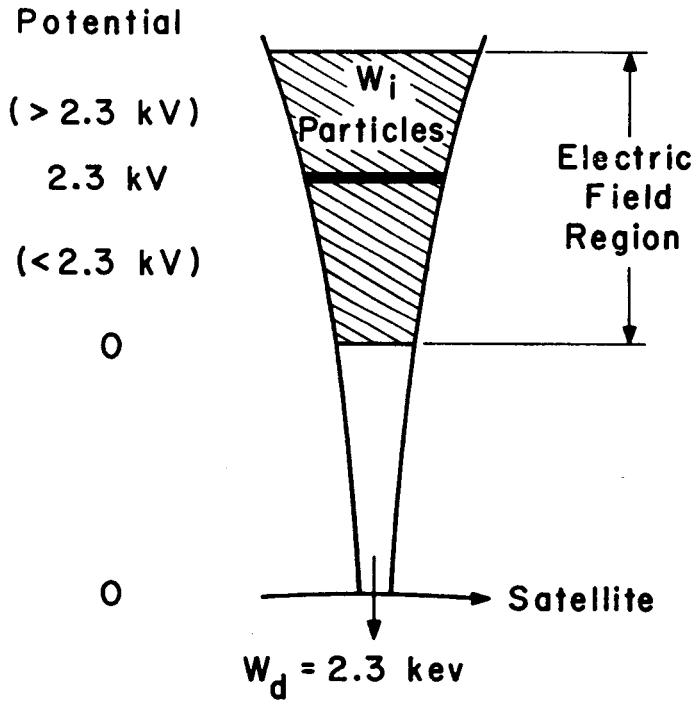
Potential
(> 2.3 kV)
2.3 kV
(< 2.3 kV)
0
0
W_i Particles
Electric Field Region
Satellite
W_d = 2.3 kev

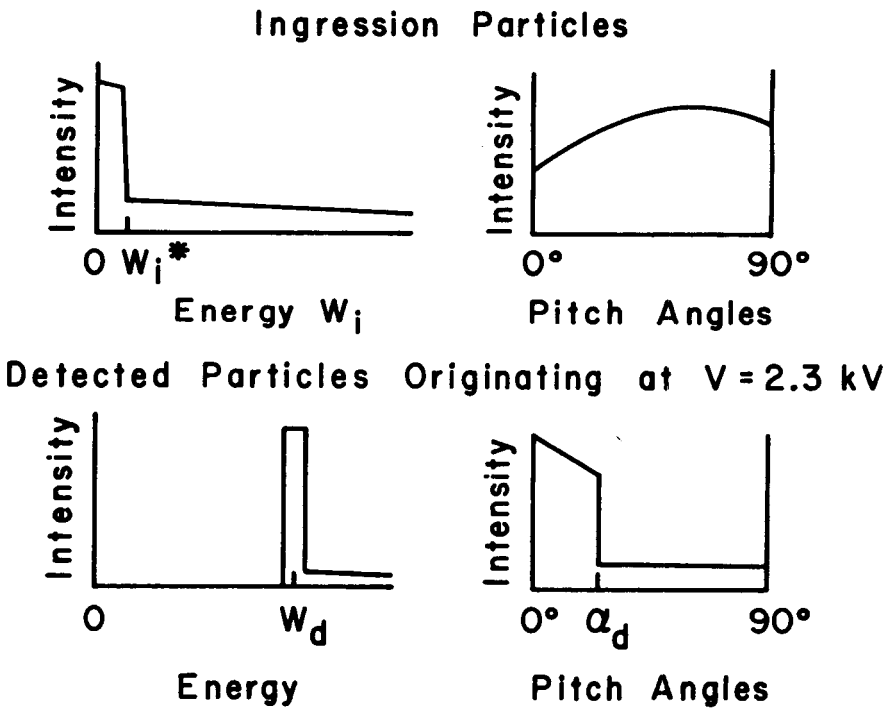
Ingression Particles
Intensity
0 W_i*
Energy W_i
Intensity
0°
90°
Pitch Angles
Detected Particles Originating at V = 2.3 kV
Intensity
0
W_d
Energy
Intensity
0° α_d
90°
Pitch Angles

Figure 15